Engineering Chemically-Active Defects in Monolayer MoS_2 Transistors *via* Ion-Beam Irradiation and Their Healing *via* Vapor Deposition of Alkanethiols

Simone Bertolazzi,[1] *Sara Bonacchi,*[1] *Guangjun Nan,*[2] *Anton Pershin,*[2] *David Beljonne*[2] *and Paolo Samorì*[1*]

[1] Dr. S. Bertolazzi, Dr. S. Bonacchi, Prof. P. Samorì
University of Strasbourg, CNRS, ISIS UMR 7006, 8 allée Gaspard Monge, F-67000 Strasbourg, France.
E-mail: samori@unistra.fr

[2] Dr. G. Nan, Dr. A. Pershin, Dr. D. Beljonne
Laboratory for Chemistry of Novel Materials
Université de Mons
Place du Parc 20, 7000 Mons, Belgium

Keywords: monolayer MoS_2, field-effect transistors, ion-beam irradiation, sulfur vacancies, thiol chemistry.

Atomically-thin semiconductors from the family of transition metal dichalcogenides (TMDCs) ─ such as monolayers of MoS_2, WS_2, $MoSe_2$ and WSe_2 ─ have been the subject of intense research efforts over the last five years, owing to their sizeable direct bandgap (1-3 eV), high charge-carrier mobility (up to ~100 $cm^2V^{-1}s^{-1}$) and excellent mechanical flexibility that make them attractive components for application in next-generation flexible (opto-) electronics.[1] Among these newly emerging two-dimensional (2D) semiconductors, monolayer MoS_2 is the prototypical and most investigated to date,[2] being the first to be used as active layer in electronic switches[3] and optoelectronic devices, such as photodetectors and solar cells.[4] Moreover, recent advances in the large-area growth of 2D MoS_2 crystals by chemical vapor deposition (CVD) have enabled a large number of studies focused on this promising material.[5] However, before such impressive pace, research on MoS_2 has been carried out for more than 50 years,[6] with relevant experiments conducted in the area of lubrication[7] and catalysis.[8] The catalytic properties of monolayer MoS_2 have also been the subject of renovated attention. It was recently demonstrated that the inert MoS_2 basal plane

could be successfully activated and optimized through the introduction of chemically-active defects (i.e. sulfur vacancies) together with strain, resulting in greatly enhanced catalytic activity for hydrogen evolution reaction (HER).[9] Sulfur vacancies are known to be present in both CVD-grown and mechanically exfoliated MoS_2 sheets,[10] but their density has to be increased and systematically controlled to promote/tune the catalytic activity of the 2D material. Various approaches have been reported in the literature for modulating the density of sulfur vacancies, namely electron irradiation,[11] thermal annealing,[12] plasma treatments,[9, 13] as well bombardment with charged particles.[14] The development of such methods is highly desirable also in the context of chemical functionalization of 2D MoS_2,[15] which is currently under intense investigation for tailoring the material properties ─ such as electronic doping and optical emission/adsorption ─ to fit the specific requirements of the different applications envisioned for this 2D semiconductor.[16] In this framework, various groups have reported that sulfur vacancies, intrinsic or created with a suitable technique, act as anchoring sites for the covalent attachment of small molecules to the surface of MoS_2 *via* thiol functional groups, enabling a remarkable tuning of its electronic, optical and vibrational properties.[12b, 17] Under this perspective, both the implementation of a sound method to control the density of sulfur vacancies and a thorough characterization of their effects on the properties of the 2D sheet are mandatory. In particular, in view of possible applications of chemically-functionalized monolayer MoS_2 in electronic devices, such as chemical (bio-)sensors,[18] it is of great interest to establish a correlation between the density of sulfur vacancies and the electronic properties of the 2D material. To the best of our knowledge, there are no reports in the literature concerning the measurement of critical field-effect device parameters (e.g. charge-carrier mobility) as a function of sulfur-vacancy density (V_S). In this work, we focus our attention on the use of low-energy Ar-ion bombardment[14b] to controllably introduce sulfur vacancies in monolayer MoS_2 sheets serving as channel material in back-gated field-effect transistors (FETs). With this approach, we can systematically

explore the changes in the electrical characteristics of our FETs with the increasing number of ions impinging on the channel surface, corresponding to a well-defined amount of newly generated sulfur vacancies. We show that the electron field-effect mobility μ_{FE} decreases as $\sim 1/V_S^2$ with increasing density of vacancies up to $V_S \approx 5\%$, in line with predictions from a Coulomb impurity scattering model. Moreover, for $V_S \geq 20\%$ our transistors display ambipolar behavior, which is consistent with the reduction of energy bandgap predicted by density functional theory (DFT) electronic structure calculations. We also demonstrate that the electrical properties can be largely recovered by exposing the ion-irradiated devices to vapors of short linear molecules with thiol headgroups, such as butanethiols, confirming previous results on defect healing *via* chemisorption of thiol-terminated molecules at sulfur vacancies.[17, 19] However, the use of vapors rather than the common solution processing with ethanol was found to be critical to evaluate the efficacy of the thiol-chemistry treatment. Besides the charge transport study, this work is complemented with a systematic characterization of ion-irradiated and thiol-treated monolayer MoS_2 sheets by means of Raman and photoluminescence (PL) spectroscopy, which further supports the conclusions.

Figure 1a shows the schematics of the ion bombardment experiment, where the channel of a back-gated monolayer MoS_2 FET is exposed to a beam of Ar^+ ions. The bombardment is carried out under high vacuum ($\sim 10^{-8}$ mbar) by means of a Thermo Fischer EX06 ion gun with acceleration voltage set at 500 V (see Methods). Previous X-ray photoemission spectroscopy (XPS) studies (ref. [14b]) demonstrated that bombarding monolayer MoS_2 films with Ar^+ ions with kinetic energy of ~500 eV allows selective removal of sulfur atoms without affecting the concentration of molybdenum atoms. We performed similar *in situ* XPS experiments (Supporting Information - Section 1) to evaluate the density of sulfur vacancies V_S generated by our ion-bombardment procedure. For an ion fluence $F \approx 8.2 \times 10^{12}$ ions·cm^{-2}, the density of generated sulfur vacancies was found to be $V_S \approx 2.3 \times 10^{13}$ cm^{-2}, which corresponds to a relative change in the sulfur content $\Delta S/S \approx -1\%$. We point out here that V_S

is intended as the density of sulfur vacancies *induced* by the bombardment process and it is assumed for simplicity that the amount of vacancies in the pristine (not bombarded) material is comparatively negligible. After obtaining the relationship between F and V_S (**Figure S2**), we proceeded to bombard our monolayer MoS_2 FETs with a variable fluence of Ar^+ ions. The experiment was carried out in multiple bombardment steps; at each step the devices were irradiated with an incremental fluence $\Delta F \approx 8.2 \times 10^{12}$ ions·cm^{-2} ─ in order to reduce the relative sulfur content by ~1% ─ and were subsequently taken out from the vacuum chamber and electrically characterized under N_2 atmosphere. The devices were not exposed to ambient air between ion bombardment and electrical measurements (see Methods). **Figure 1**b displays a typical set of transfer curves (drain-source current I_{ds} *vs* gate voltage V_g) measured on the same monolayer MoS_2 FET at different steps of the ion-bombardment process. It can be seen that the ON-current level decreases monotonically with V_S and the switching capability of the transistor becomes gradually compromised. **Figure 1**c compares the PL spectra of a mechanically-exfoliated monolayer MoS_2 flake acquired for different values of ion fluence (equivalently V_S). The panel inset displays the intensities of the A and B exciton peaks as a function of V_S, which decrease exponentially and cross each other at $V_S \approx 5.2\%$ (corresponding to a fluence $F \approx 4.3 \times 10^{13}$ ions·cm^{-2}). Furthermore, we noticed the occurrence of a slight blue shift for both A and B exciton peaks, as well as the development of a sub-bandgap PL-emission peak at $E_d \approx 1.75$ eV (**Figure S10**). Defect-induced PL emission in semiconducting TMDCs has been previously investigated,[14a] revealing the emergence of a new peak (1.78 eV) in the PL spectra of monolayer MoS_2 sheets irradiated with α particles or thermally annealed at ~500 °C in order to create sulfur vacancies; the peak was attributed to the radiative recombination of neutral excitons bound to defect states. The evolution of the two main Raman-active phonon modes ─ namely the polar E′ and the homopolar A'_1 optical phonon modes ─ is presented in **Figure 1**d. The most remarkable features are the blue (red) shift of the A'_1 (E′) mode, displayed in the panel inset, as well as the development of two

disorder-activated Raman bands (ref. [20]) at frequencies higher and lower than the A'_1 and E′ peaks, respectively.

The devices fabricated in this work exhibited a two-terminal electron field-effect mobility μ_{FE} within the range 10-30 $cm^2V^{-1}s^{-1}$, whereas the mobility extracted using the four-terminal measurement configuration ranged between 20 and 40 $cm^2V^{-1}s^{-1}$, approaching the values obtained with unencapsulated FETs on SiO_2/Si substrates in high-vacuum conditions.[21] The measurements were in fact carried out using both two-probe and four-probe configurations (see Supporting Information - Section 2.1) to confirm that the changes in the electrical characteristics of the ion-irradiated FETs stemmed from the transistor channel itself and not from variations in the contact resistance. **Figure 2**a portrays the two-terminal transfer characteristics of a typical monolayer MoS_2 FET that underwent the ion-bombardment procedure. After irradiating the device with an ion fluence $F \approx 8.2 \times 10^{12}$ ions·cm^{-2} (i.e. $\Delta S/S \approx -1\%$) the mobility μ_{FE} drops from ~25 $cm^2V^{-1}s^{-1}$ to ~8 $cm^2V^{-1}s^{-1}$ while the threshold voltage V_{th} shifts towards positive V_g values by an amount $\Delta V_{th} \approx +20.5$ V, which corresponds to a change in the carrier density $\Delta n_{th} \approx 1.5 \times 10^{12}$ cm^{-2}. The positive shift of V_{th} indicates that newly created defect states have to be filled before reaching the linear regime of the I_{ds} *vs* V_g transfer curves associated with conduction-band transport. Defect states are responsible for reducing the fraction of mobile carriers in the conduction band; at the same time they increase the fraction of trapped carriers that do not contribute to charge transport, resulting in a degraded effective mobility.[22] In agreement with previous reports,[17c] we found that the sulfur vacancies act as trap states, as it can be inferred by considering that Δn_{th} scales with the amount of vacancies introduced with ion bombardment. In fact, with further increase of V_S, the threshold voltage V_{th} was found to shift towards larger positive values, as shown in the panel inset. For $V_S \geq 3\%$ an unambiguous linear regime could not be identified within the gate-voltage range used in the experiment, which is the reason behind the saturation appearing in the V_{th} *vs* V_S plot (inset, **Figure 2**a). To elucidate the exact nature of charge transport at various

levels of disorder, temperature-dependent studies ought to be performed, which is however beyond the scope of the present work. We rather resorted to modeling. Based on DFT electronic structure calculations of pristine MoS_2 monolayers, we applied the semi-classical Boltzmann transport theory in the relaxation time approximation, including scattering by both phonons and Coulomb impurities (CI) generated by charge filling at sulfur vacancies (see Supporting Information - Section 5). The band electron mobility values were corrected to account for the non-linear dependence of mobile, free, charge carriers with gate voltage, as previously proposed (ref. [22]). The resulting field-effect mobilities, reported in **Figure 2**b (white circles), show a power-law dependence with the concentration of sulfur vacancies ($\mu_{FE} \propto V_S^{-\gamma}$) with a falloff parameter γ close to 2 (γ = 1.93). Such an evolution arises from the combined effect of CI scattering and the free versus total charge density renormalization factor, both scaling as $1/V_S$. **Figure 2**b displays the experimental mobilities (blue circles) obtained from linear fitting of the two-terminal transfer curves in the high positive gate-voltage range (70-90 V). When using in the charge transport simulations a total electron density of 1.5×10^{13} cm^{-2} ─ in line with Hall-effect measurements[23] performed on back-gated FETs with similar oxide thickness and high *n*-doping level ─ a satisfactory agreement is found between theory and experiment for V_S values up to 5%. Instead, beyond 5% the predicted mobilities largely exceed the experimental data, likely suggesting a breakdown of the band model used here and the predominance of hopping transport. For $V_S \geq 10\%$, the experimental μ_{FE} forms a plateau at $\sim2\times10^{-4}$ $cm^2V^{-1}s^{-1}$ and I_{ON}/I_{OFF} becomes definitively smaller than 10, indicating the almost complete loss of the device switching capability. At the same time, new interesting features can be observed in the transfer characteristics, see **Figure 2**c. Firstly, with increasing V_S, the curves undergo a vertical shift in the graph, i.e. the overall conductivity of the 2D MoS_2 sheet increases due to the larger amount of localized defect states available for hopping-type charge transport. Secondly, for $V_S \geq 20\%$, the FETs display ambipolar

behavior, where the *p*-type mobility increases with V_S and matches the *n*-type counterpart at $V_S \approx 35\%$ (**Figure 2**d). This suggests the occurrence of a rearrangement in the band structure of the 2D semiconductor associated with a reduction of its bandgap, as demonstrated by DFT electronic structure calculations for sulfur vacancy contents ranging from 0 up to 25% (see Supporting Information - Section 6).

After elucidating the influence of ion-beam induced sulfur vacancies on the electrical transport properties of monolayer MoS_2, we explored the efficacy of chemical treatments with thiol molecules. Here we used one among the shortest thiol-terminated linear molecules, namely butanethiol ($C_4H_{10}S$ ─ **Figure 3**a). The chain length was minimized in order to promote the edge-on surface-molecule orientation, with the aim of (i) reducing the steric hindrance hampering the filling of neighboring sulfur vacancies, and (ii) minimize the electronic coupling of the molecule with the MoS_2 surface, which is expected to act as a source of electronic disorder detrimental for charge transport. In a first attempt, we performed the chemical treatment using previously published methods based on solutions of thiol molecules in ethanol.[12b, 17b] However, control experiments carried out only in the presence of neat ethanol (anhydrous, ≤ 0.003% water) unexpectedly revealed a non-negligible recovery of the electrical characteristics of the ion-irradiated FETs (see Supporting Information - Section 2.4). Such finding is nevertheless very reasonable since oxygen and sulfur are valence isoelectronic atoms, and oxygen-containing molecules can also contribute to defect healing *via* strong chemical interaction with unsaturated molybdenum atoms.[24] Moreover, the presence of multiple sulfur vacancies, which are likely to be generated during Ar-ion bombardment,[25] could increase significantly the reactivity of the MoS_2 basal plane with such molecular species. Therefore, we implemented a vapor-phase treatment to exclude secondary healing mechanisms (see Methods). In parallel, control experiments were performed with vapors of pentane (C_5H_{12} ─ see **Figure S9**), which were not found to improve/recover the devices' electrical properties. First, we show the effects induced by butanethiol molecules on the transfer characteristics of pristine FETs

(**Figure 3**b). The treatment with short thiol molecules augments the ON-current level, reduces the hysteresis and increases the field-effect mobility (from ~21 to ~33 $cm^2V^{-1}s^{-1}$), which is consistent with the reduction of charged traps associated with sulfur vacancies in the pristine MoS_2 sheets. Conversely, the use of long alkanethiol molecules, such as hexadecanethiol ($HS(CH_2)_{15}CH_3$), was reported to reduce both the charge-carrier mobility and the ON current level.[17b] Afterwards, we tested the efficacy of our method on ion-irradiated devices with a density of generated vacancies $V_S \approx 3\%$. **Figure 3**c shows the effects on the transfer characteristics: after treatment (green circles) a remarkable recovery was obtained from the degraded condition set by ion bombardment (light-blue circles). The butanethiol treatment enhanced the I_{ON}/I_{OFF} ratio from ~2×10^6 to ~4×10^7 and the field-effect mobility from ~1.4 to ~8.0 $cm^2V^{-1}s^{-1}$. Using the power-law trend $\mu_{FE} \propto V_S^{-\gamma}$ we could estimate a sulfur-vacancy density post treatment of ~1.2%, which represents a clear improvement over the pre-treatment condition ($V_S \approx 3\%$). PL and Raman spectroscopy measurements display as well signatures of defect healing. **Figure 4**a compares the PL spectra of an ion-irradiated MoS_2 sheet, before and after exposure to butanethiol vapors. Upon treatment, both A and B exciton peaks red shift (10-20 meV), the defect-mediated emission peak at $E_d \approx 1.75$ eV remarkably decreases whereas the A exciton peak increases. At the same time, the Raman spectra (**Figure 4**b) show a damping of the disorder-activated side bands together with a blue shift and red shift of the E′ and A'_1 peaks, respectively, consistent with the reduction of sulfur vacancies (see **Figure 1**d for comparison). Finally, control experiments were performed with vapors of an analogous molecule without thiol anchoring group i.e., pentane (C_5H_{12} ─ see **Figure S9**) and, importantly, we found no trace of improvement/recovering of the devices' electrical properties.

In summary, we demonstrated that low-energy Ar-ion irradiation can be effectively employed to create sulfur vacancies in 2D sheets of MoS_2 enabling a systematic control over defect density. Ion beams can be rastered over centimeter-scale large areas in relatively short times ─ as

compared to their electron counterpart ─ and could be further adapted for direct patterning of defective regions in CVD-grown films of MoS_2, which would not be feasible with thermal annealing or plasma treatments that act on the entire sample surface. For the first time to our knowledge, the effects of ion-beam generated sulfur vacancies on the electrical characteristics of monolayer MoS_2 FETs were elucidated by establishing a correlation between critical device parameters and the density of generated sulfur vacancies. Moreover, we employed a new chemical treatment based on vapors of short thiol-terminated molecules that allowed improving the electrical properties of pristine FETs and enabled a significant recovery of the performance of ion-irradiated FETs. Our solvent-free procedure ─ carried out strictly under inert atmosphere ─ rules out secondary healing effects by oxygen or oxygen-containing molecules, such as ethanol, and could be further exploited to functionalize 2D MoS_2 sheets with a virtually-infinite number of molecules possessing thiol functional groups. Our findings represent a guideline for the trade-off choice between electronic device performance and density of chemically-active defects suitable for chemical functionalization.

Experimental Section

Ion bombardment: Ar-ion bombardment of monolayer MoS_2 FETs was performed by means of a Thermo Fischer EX06 ion gun with acceleration voltage of 500 V. The angle between the ion beam and the substrate surface normal was ~ 58°. To avoid shadow effects due to the metal contact thickness, the FETs were oriented with their channel-width direction parallel to the projection of the ion beam on the sample surface. The ion-beam (I ~ 210 nA) was uniformly raster-scanned over a rectangular area of ~ 8 × 4 mm^2 (see Supporting Information - Section 1).

Device fabrication and electrical characterization: Monolayer MoS_2 flakes were mechanically exfoliated with from commercially available molybdenite crystals (Furuchi, Japan) and were identified through a combination of optical microscopy, Raman and PL spectroscopy. Back-gated FETs with two-probe and four-probe geometry were fabricated on thermally oxidized

heavily *n*-doped silicon substrates (ρ_{Si} ~ 0.001 Ω·cm, t_{ox} = 290 nm) by means of e-beam lithography with a double-layer of polymethyl methacrylate (PMMA), thermal evaporation of Au (85 nm) and lift-off in warm acetone (~50 °C). As-fabricated devices were annealed at 140 °C for ~15 hours inside a high-vacuum chamber (~5×10^{-8} mbar) to reduce contact resistance and desorb atmospheric adsorbates.[26] Importantly, the FETs were no longer exposed to air after annealing and were electrically characterized only under inert atmosphere (N_2-filled glovebox). Electrical measurements were carried out at room temperature with source-measurement units from Keithley (model 2636A).

Raman and photoluminescence spectroscopy: Raman and PL spectra were acquired at room temperature with a Renishaw InVia spectrometer equipped with a 532 nm laser. The measurements were carried in air out using a 100× lens objective (numerical aperture NA = 0.85) providing a beam spot size of ~700 nm. The excitation power was kept below 1 mW to avoid local heating damage effects. For Raman (PL) measurements, the wavenumber (energy) resolution was ~1.25 cm^{-1} (~1 meV). The continuous-lines Raman spectra are obtained with the cardinal spline interpolation method. The Si band at 520.3 cm^{-1} was used for normalization.

Chemical treatment with butanethiol vapors: The substrates holding the FETs were fixed onto the lid of a 20 ml glass container filled with 200 µl of 1-butanethiol (99%, Sigma Aldrich). The lid was closed ─ with the sample surface facing the liquid ─ and the container was saturated with butanethiol vapor by heating for 3 hours at 70 °C. The samples were then placed on a hot plate and annealed for 1 hour at 70 °C to remove non-chemisorbed molecules. All the process was carried out under inert atmosphere (N_2-filled glovebox).

Supporting Information

Supporting Information is available from the Wiley Online Library or from the author.

Acknowledgements

We thank E. Orgiu, A. Galanti and M. Squillaci (ISIS) for valuable discussions, T. Carney (Thermo Fisher Scientific Inc.) for precious support with the ion gun settings, Z. Shuai and T. Zhao (Tsinghua University) for help with the charge transport simulations, and F. Richard (ISIS) for recording the XPS spectra. Device fabrication was carried out in part at the nanotechnology facility STNano (IPCMS) with the assistance of S. Siegwald. We acknowledge funding from the M-ERA.NET project MODIGLIANI, the European Commission through the Graphene Flagship (GA-696656) and the Marie-Curie IEF MULTI2DSWITCH (GA-700802), the Agence Nationale de la Recherche through the LabEx project Chemistry of Complex Systems (ANR-10- LABX-0026_CSC) and the International Center for Frontier Research in Chemistry (icFRC). The work in Mons is supported by BELSPO through the PAI P6/27 Functional Supramolecular Systems project, by the Belgian National Fund for Scientific Research FNRS/F.R.S and by the Marie-Curie IEF DEMONH (SEP.210205877). DB is a Research Director of FNRS.

References

[1] a) Q. H. Wang, K. Kalantar-Zadeh, A. Kis, J. N. Coleman, M. S. Strano, *Nat. Nanotechnol.* **2012**, *7*, 699; b) G. Fiori, F. Bonaccorso, G. Iannaccone, T. Palacios, D. Neumaier, A. Seabaugh, S. K. Banerjee, L. Colombo, *Nat. Nanotechnol.* **2014**, *9*, 768.

[2] O. V. Yazyev, A. Kis, *Mater. Today* **2015**, *18*, 20.

[3] B. Radisavljevic, A. Radenovic, J. Brivio, V. Giacometti, A. Kis, *Nat. Nanotechnol.* **2011**, *6*, 147.

[4] D. Lembke, S. Bertolazzi, A. Kis, *Acc. Chem. Res.* **2015**, *48*, 100.

[5] a) Y. Shi, H. Li, L.-J. Li, *Chem. Soc. Rev.* **2015**, *44*, 2744; b) Y. L. Huang, Y. Chen, W. Zhang, S. Y. Quek, C.-H. Chen, L.-J. Li, W.-T. Hsu, W.-H. Chang, Y. J. Zheng, W. Chen, A. T. S. Wee, *Nat. Commun.* **2015**, *6*, 6298; c) D. Dumcenco, D. Ovchinnikov, K. Marinov, P. Lazić, M. Gibertini, N. Marzari, O. L. Sanchez, Y.-C. Kung, D. Krasnozhon, M.-W. Chen, S. Bertolazzi, P. Gillet, A. Fontcuberta i Morral, A. Radenovic, A. Kis, *ACS Nano* **2015**, *9*, 4611.

[6] R. F. Frindt, *J. Appl. Phys.* **1966**, *37*, 1928.

[7] a) P. D. Fleischauer, R. Bauer, *Tribol. Trans.* **1988**, *31*, 239; b) M. Chhowalla, G. A. J. Amaratunga, *Nature* **2000**, *407*, 164.

[8] a) C. B. Roxlo, H. W. Deckman, J. Gland, S. D. Cameron, R. R. Chianelli, *Science* **1987**, *235*, 1629; b) T. F. Jaramillo, K. P. Jørgensen, J. Bonde, J. H. Nielsen, S. Horch, I. Chorkendorff, *Science* **2007**, *317*, 100; c) R. R. Chianelli, M. H. Siadati, M. P. De la Rosa, G. Berhault, J. P. Wilcoxon, R. Bearden, B. L. Abrams, *Catal. Rev. Sci. Eng.* **2006**, *48*, 1.

[9] H. Li, C. Tsai, A. L. Koh, L. Cai, A. W. Contryman, A. H. Fragapane, J. Zhao, H. S. Han, H. C. Manoharan, F. Abild-Pedersen, J. K. Nørskov, X. Zheng, *Nat. Mater.* **2016**, *15*, 48.

[10] a) W. Zhou, X. Zou, S. Najmaei, Z. Liu, Y. Shi, J. Kong, J. Lou, P. M. Ajayan, B. I. Yakobson, J.-C. Idrobo, *Nano Lett.* **2013**, *13*, 2615; b) H. Qiu, T. Xu, Z. Wang, W. Ren, H. Nan, Z. Ni, Q. Chen, S. Yuan, F. Miao, F. Song, G. Long, Y. Shi, L. Sun, J. Wang, X. Wang, *Nat. Commun.* **2013**, *4*, 2642; c) J. Hong, Z. Hu, M. Probert, K. Li, D. Lv, X. Yang, L. Gu, N. Mao, Q. Feng, L. Xie, J. Zhang, D. Wu, Z. Zhang, C. Jin, W. Ji, X. Zhang, J. Yuan, Z. Zhang, *Nat. Commun.* **2015**, *6*, 6293.

[11] W. M. Parkin, A. Balan, L. Liang, P. M. Das, M. Lamparski, C. H. Naylor, J. A. Rodríguez-Manzo, A. T. C. Johnson, V. Meunier, M. Drndić, *ACS Nano* **2016**, *10*, 4134.

[12] a) M. Donarelli, F. Bisti, F. Perrozzi, L. Ottaviano, *Chem. Phys. Lett.* **2013**, *588*, 198; b) D. M. Sim, M. Kim, S. Yim, M.-J. Choi, J. Choi, S. Yoo, Y. S. Jung, *ACS Nano* **2015**, *9*, 12115.

[13] B. Peng, G. Yu, Y. Zhao, Q. Xu, G. Xing, X. Liu, D. Fu, B. Liu, J. R. S. Tan, W. Tang, H. Lu, J. Xie, L. Deng, T. C. Sum, K. P. Loh, *ACS Nano* **2016**, *10*, 6383.

[14] a) S. Tongay, J. Suh, C. Ataca, W. Fan, A. Luce, J. S. Kang, J. Liu, C. Ko, R. Raghunathanan, J. Zhou, F. Ogletree, J. Li, J. C. Grossman, J. Wu, *Sci. Rep.* **2013**, *3*, 2657; b) Q. Ma, P. M. Odenthal, J. Mann, D. Le, C. S. Wang, Y. Zhu, T. Chen, S. Dezheng, K. Yamaguchi, T. Tran, M. Wurch, J. L. McKinley, J. Wyrick, K. Magnone, T. F. Heinz, T. S. Rahman, R. Kawakami, L. Bartels, *J. Phys. Condens. Matter* **2013**, *25*, 252201; c) Q. Ma, M.

Isarraraz, C. S. Wang, E. Preciado, V. Klee, S. Bobek, K. Yamaguchi, E. Li, P. M. Odenthal, A. Nguyen, D. Barroso, D. Sun, G. von Son Palacio, M. Gomez, A. Nguyen, D. Le, G. Pawin, J. Mann, T. F. Heinz, T. S. Rahman, L. Bartels, *ACS Nano* **2014**, *8*, 4672.

[15] a) D. Voiry, A. Goswami, R. Kappera, C. D. C. C. E. Silva, D. Kaplan, T. Fujita, M. Chen, T. Asefa, M. Chhowalla, *Nat. Chem.* **2015**, *7*, 45; b) S. Presolski, M. Pumera, *Mater. Today* **2016**, *19*, 140; c) X. Chen, A. R. McDonald, *Adv. Mater.* **2016**, *28*, 5738.

[16] C. R. Ryder, J. D. Wood, S. A. Wells, M. C. Hersam, *ACS Nano* **2016**, *10*, 3900.

[17] a) E. P. Nguyen, B. J. Carey, J. Z. Ou, J. van Embden, E. D. Gaspera, A. F. Chrimes, M. J. S. Spencer, S. Zhuiykov, K. Kalantar-zadeh, T. Daeneke, *Adv. Mater.* **2015**, *27*, 6225; b) K. Cho, M. Min, T.-Y. Kim, H. Jeong, J. Pak, J.-K. Kim, J. Jang, S. J. Yun, Y. H. Lee, W.-K. Hong, T. Lee, *ACS Nano* **2015**, *9*, 8044; c) Z. Yu, Y. Pan, Y. Shen, Z. Wang, Z.-Y. Ong, T. Xu, R. Xin, L. Pan, B. Wang, L. Sun, J. Wang, G. Zhang, Y. W. Zhang, Y. Shi, X. Wang, *Nat. Commun.* **2014**, *5*, 5290.

[18] a) J.-S. Kim, H.-W. Yoo, H. O. Choi, H.-T. Jung, *Nano Lett.* **2014**, *14*, 5941; b) D. Sarkar, W. Liu, X. Xie, A. C. Anselmo, S. Mitragotri, K. Banerjee, *ACS Nano* **2014**, *8*, 3992.

[19] M. Makarova, Y. Okawa, M. Aono, *J. Phys. Chem. C* **2012**, *116*, 22411.

[20] S. Mignuzzi, A. J. Pollard, N. Bonini, B. Brennan, I. S. Gilmore, M. A. Pimenta, D. Richards, D. Roy, *Phys. Rev. B* **2015**, *91*, 195411.

[21] a) D. Lembke, A. Allain, A. Kis, *Nanoscale* **2015**, *7*, 6255; b) D. Jariwala, V. K. Sangwan, D. J. Late, J. E. Johns, V. P. Dravid, T. J. Marks, L. J. Lauhon, M. C. Hersam, *Appl. Phys. Lett.* **2013**, *102*, 173107

[22] W. Zhu, T. Low, Y.-H. Lee, H. Wang, D. B. Farmer, J. Kong, F. Xia, P. Avouris, *Nat. Commun.* **2014**, *5*, 3087.

[23] B. W. H. Baugher, H. O. H. Churchill, Y. Yang, P. Jarillo-Herrero, *Nano Lett.* **2013**, *13*, 4212.

[24] a) J. Lu, A. Carvalho, X. K. Chan, H. Liu, B. Liu, E. S. Tok, K. P. Loh, A. H. Castro Neto, C. H. Sow, *Nano Lett.* **2015**, *15*, 3524; b) D. Ma, Q. Wang, T. Li, C. He, B. Ma, Y. Tang, Z. Lu, Z. Yang, *J. Mater. Chem. C* **2016**, *4*, 7093; c) Y. Liu, P. Stradins, S.-H. Wei, *Angew. Chem. Int. Ed.* **2016**, *55*, 965.

[25] a) A. Inoue, T. Komori, K.-I. Shudo, *J. Electron. Spectrosc. Relat. Phenom.* **2013**, *189*, 11; b) J. B. Park, C. B. France, B. A. Parkinson, *J. Vac. Sci. Technol. B* **2005**, *23*, 1532; c) S. Naohisa, O. Keiichi, *Jpn. J. Appl. Phys.* **1995**, *34*, 3363.

[26] S.-L. Li, K. Tsukagoshi, E. Orgiu, P. Samorì, *Chem. Soc. Rev.* **2016**, *45*, 118.

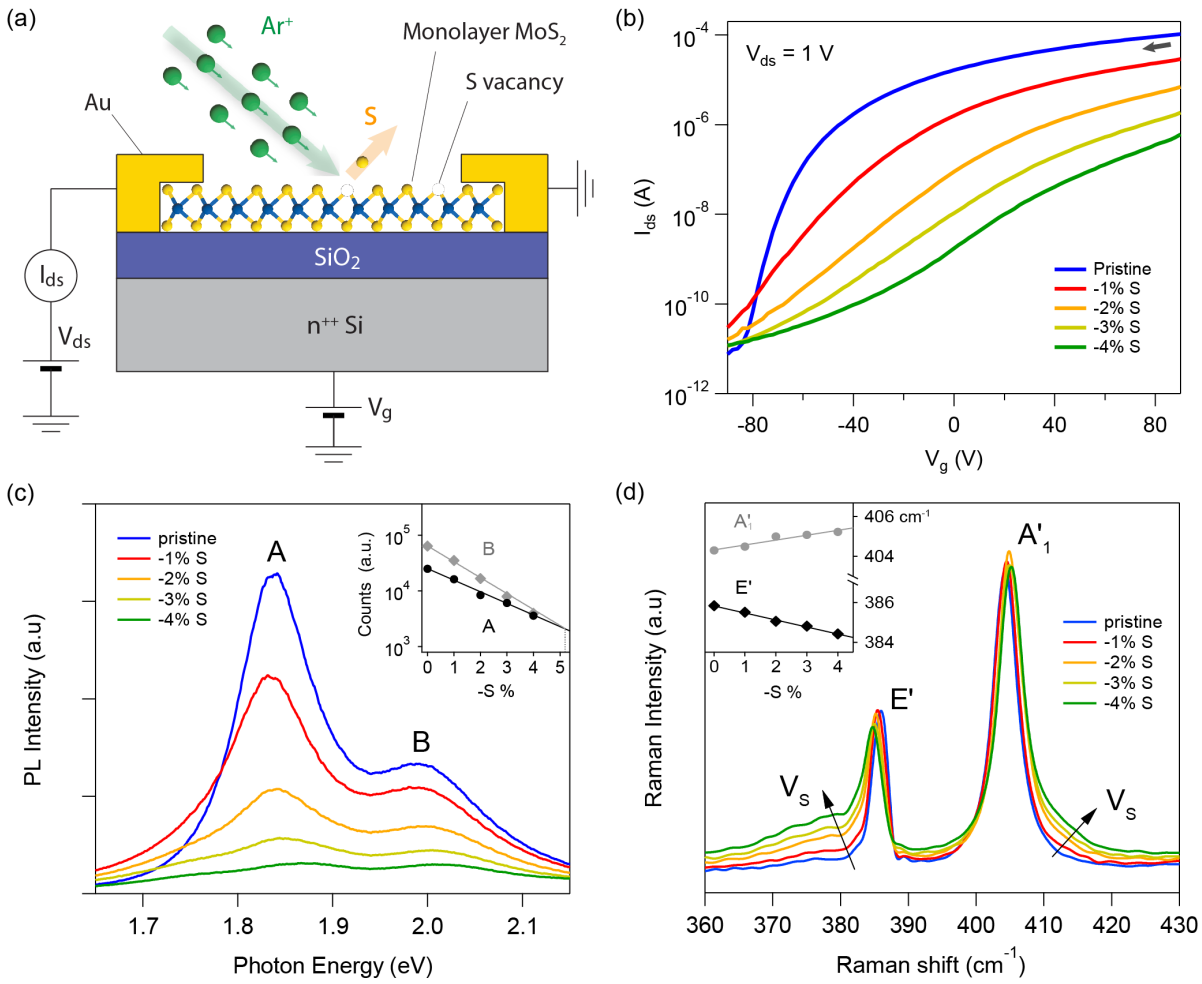

Figure 1. Effects of Ar-ion irradiation on the properties of 2D MoS_2. (a) Schematic illustration of the ion-bombardment experiment. (b) Drain-source current (I_{ds}) *vs* gate voltage (V_g) transfer characteristics of a monolayer MoS_2 FET exposed to an increasing fluence of Ar ions. The black arrow indicates the sweep direction, which was the same for all measurements. The density of generated vacancies V_S, which is expressed as percentage of decrease in the sulfur content (e.g. -1%), has been determined by XPS measurements (Supporting Section 1). (c) PL spectra of a mechanically exfoliated monolayer MoS_2 flake on SiO_2/Si for different V_S values. The inset (log-lin scale) shows the exponential decrease of the A and B exciton peak intensity with increasing V_S. (d) Raman spectra for the same flake as in (c) showing the main Raman-active phonon modes of MoS_2, as well as the development of disorder-activated side bands. The A'_1 mode blue shifts, whereas the E' mode red shifts (inset).

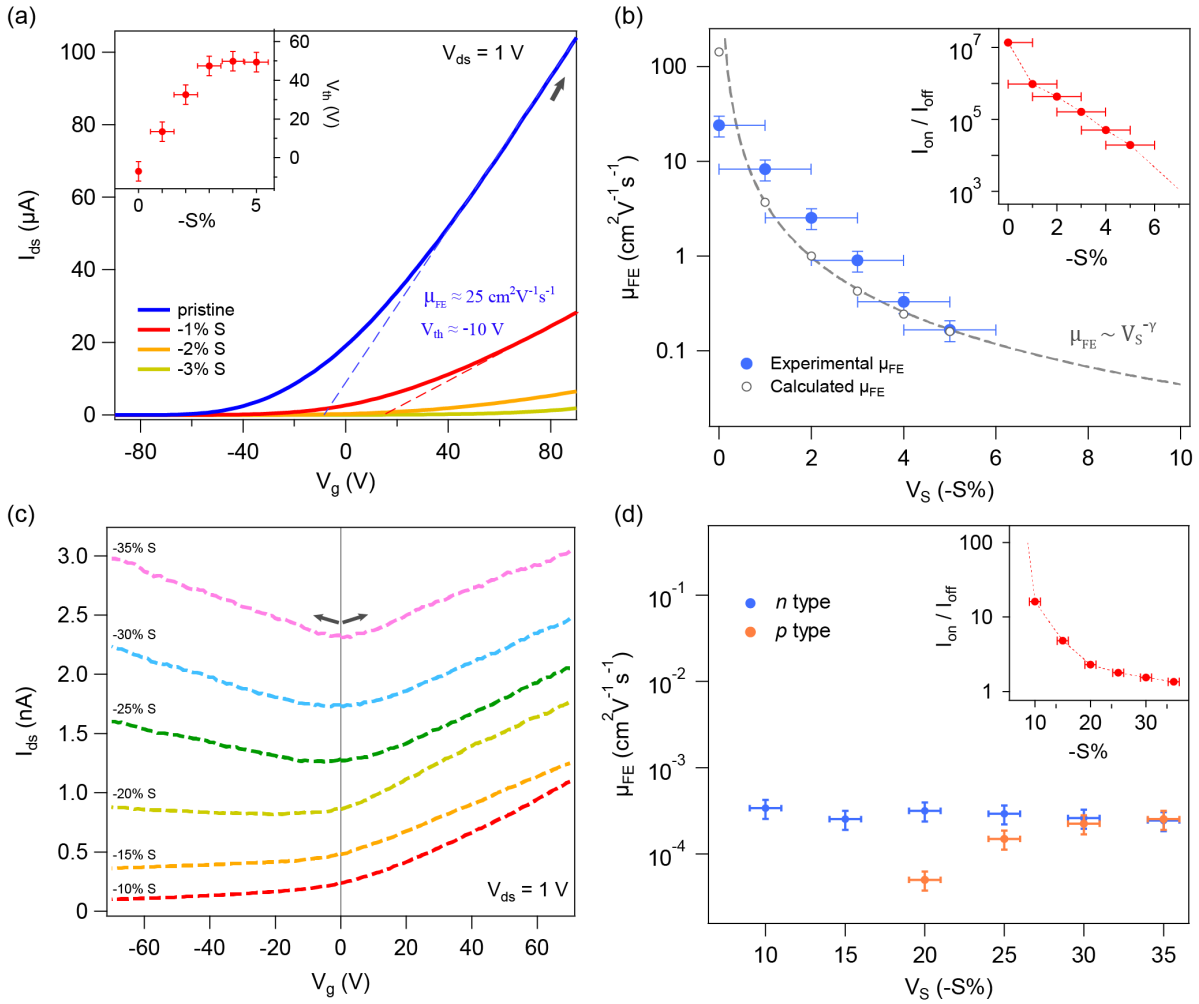

Figure 2. Impact of sulfur vacancies on charge transport. (a) Transfer characteristics (I_{ds} *vs* V_g) of a monolayer MoS_2 FET exposed to an incremental dose of Ar ions (solid lines). The dashed lines correspond to the linear fitting from which μ_{FE} and V_{th} were extracted. Inset: plot of V_{th} as a function of V_S. (b) Measured (blue circles) and calculated (white circles) μ_{FE} for V_S values up to 5%. The gray dashed line represents the power-law trend with falloff parameter $\gamma = 1.93$. Inset: plot of I_{ON}/I_{OFF} as a function of V_S. (c) Transfer curves for V_S values within the range 10-35%. To avoid slow charging/discharging effects upon application of a gate voltage bias (see Supporting Section 2.2), the curves were acquired in two steps as indicated by the arrows, gradually increasing (decreasing) the gate voltage from 0 to 90 V (-90 V). (d) Experimental *n* and *p*-type field-effect mobility for $V_S > 5\%$. Inset: I_{ON}/I_{OFF} *vs* V_S data plot. Device dimensions: L=0.8 μm and W=2.8 μm.

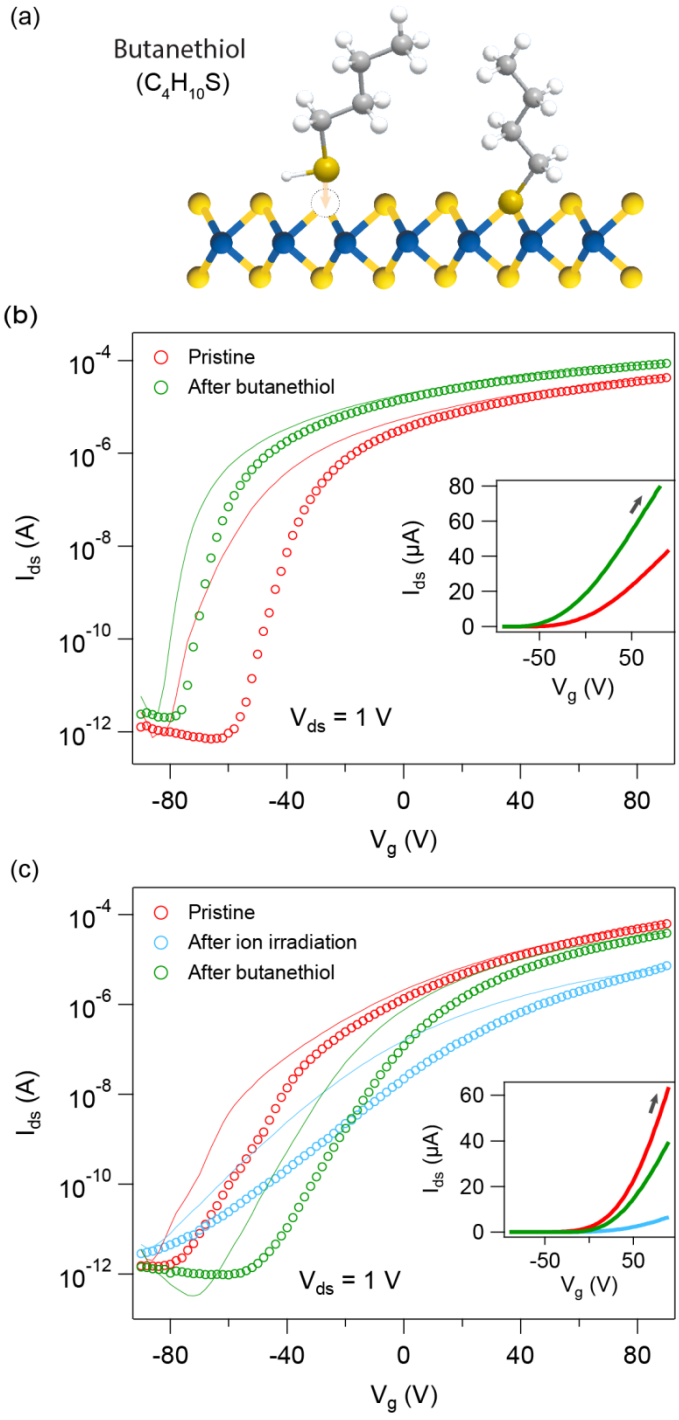

Figure 3. Charge transport in chemically-treated monolayer MoS_2 FETs. (a) Schematic drawing of the healing process: butanethiol molecules fill the sulfur vacancies *via* covalent interaction with unsaturated molybdenum atoms. (b) Transfer characteristics in log-lin scale — acquired with sweep direction from +90 V to -90 V — of a pristine monolayer MoS_2 FET before (red circles) and after (green circles) exposure to butanethiol vapors. The solid lines correspond to the opposite sweep direction and are shown also in lin-lin scale in the inset. (c) Same curves as in (b) for a device that underwent an intermediate step of ion bombardment (light-blue curves), which generated sulfur vacancies with a density $V_S \approx 3\%$.

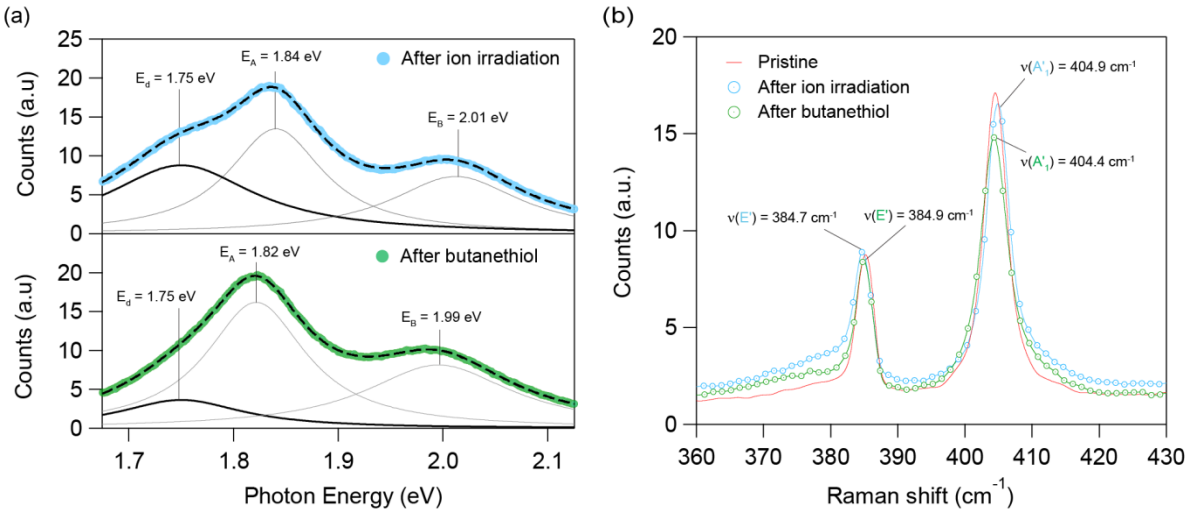

Figure 4. Effects of butanethiol on PL and Raman spectra. (a) PL spectra of a monolayer MoS_2 flake acquired after ion irradiation ($V_S \approx 3\%$, top) and after treatment with butanethiol (bottom). The spectra were fitted with a triple Lorentzian function (dashed lines) to take into account the defect-mediated emission occurring at $E_d \approx 1.75$ eV. The individual Lorentzian components are shown in solid lines. For simplicity, the A exciton/trion peak was taken as one. (b) Raman spectra of the same flake as in (a) acquired after ion irradiation (light blue) and after exposure to butanethiol vapors (green). For comparison, the spectrum of the pristine flake is also shown (red line). PL and Raman peak energies were rounded to the nearest hundredth and tenth, respectively